IEEE Access
Multidisciplinary ⋮ Rapid Review ⋮ Open Access Journal

Received 8 September 2022, accepted 22 September 2022, date of publication 28 September 2022,
date of current version 10 October 2022.

Digital Object Identifier 10.1109/ACCESS.2022.3210247

RESEARCH ARTICLE

Modeling, Analysis, and Optimization of Robotic Light Machining Tasks for Empowering Digital Twin: Generalized Impulse Model Approach

ABID IMRAN[1], SANGHWA KIM[2], JAEHONG WOO[3], AND BYUNG-JU YI[4], (Member, IEEE)

[1]Faculty of Mechanical Engineering, GIK Institute of Engineering Sciences and Technology, Swabi 23640, Pakistan
[2]Department of Electrical and Electronic Engineering, Hanyang University, Ansan 15588, South Korea
[3]Department of Robotics and Convergence, Hanyang University, Ansan 15588, South Korea
[4]School of Electrical Engineering, Hanyang University, Ansan 15588, South Korea

Corresponding authors: Jaehong Woo (jokers12@hanyang.ac.kr) and Byung-Ju Yi (bj@hanyang.ac.kr)

This work was supported in part by the Technology Innovation Program (or Industrial Strategic Technology Development Program) (Development of Robotic Work Control Technology Capable of Grasping and Manipulating Various Objects in Everyday Life Environment Based on Multimodal Recognition and Using Tools) funded by the Ministry of Trade, Industry & Energy (MOTIE, South Korea) under Grant 20001856; and in part by the BK21FOUR Program funded by the National Research Foundation of Korea (NRF).

ABSTRACT Light machining tasks by robots are becoming an important issue to replace shortages of human resources. To improve the quality, safety and overall performance of manufacturing process, the modeling for estimation of forces and torques during the machining operations is on demand. In parallel, the digital model has also been developed which allow to detect the foul conditions, save energy & time and optimization of the real manufacturing process. Digital twins are one of them which use the offline and online data to simulate the physical manufacturing process. However, the empowerment of digital twins can be improved further by developing more accurate mathematical model which allow to simulate the physical machining process in real time. Accordingly, this paper presents a formulation for the mechanics of robotic light machining tasks to empower the digital twin. In this paper, a generalized impulse model is employed to analyze a light machining task that combines the linear and angular motions. For the implementation of an impulse model-based approach, the concept of both effective mass and effective inertia is newly introduced to reflect the dynamics of the environment, which depends on the hardness of the material and process parameters (feed rate and speed (rpm) etc.) of the machining task. Furthermore, optimal feed rates are calculated with consideration of effective mass/effective inertia and minimum task completion time. Moreover, simulations are carried out to choose the feasible direction of linear and angular velocities and optimal non-singular workspace for light machining tasks. Finally, the proposed methodology is validated through a quantitative comparison of simulation and experimental results by performing the drilling and milling tasks. A 6-DOF Universal robot (UR 5e) is used for simulations and experiments to corroborate the effectiveness of the proposed algorithms for light machining tasks. The developed methodology will certainly empower the digital twin for their physical analog during light machining operations.

INDEX TERMS Digital twin, light machining, robotic drilling, robotic milling, impulse model, effective mass effective inertia.

I. INTRODUCTION

Robot manipulators certainly have dominated over human worker for industrial production due to their ability to work tirelessly with high precision, repeatability, and quality control aspect of the process [1], [2], [3], [4]. According to the International Federation of Robotics, more than 72% of industrial robots are used to replace repetitive manual labor in the field of low precision, such as pick and place, welding, and assembling tasks [5]. Now a days, the continuous

The associate editor coordinating the review of this manuscript and approving it for publication was Yangmin Li.

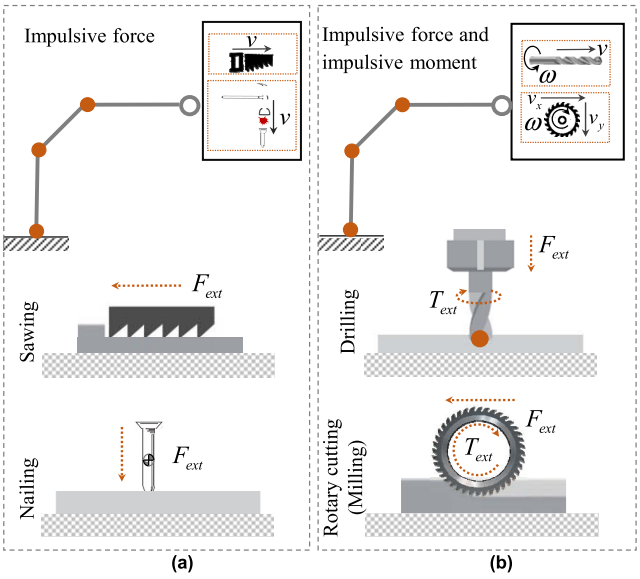

FIGURE 1. Impulsive motion-based machining tasks. (a) Linear impulsive motion- based machining task (b) Linear and angular impulsive motion-based machining tasks.

development and progress in robot technology enables the robotic systems to perform high value-added operations such as milling and drilling [6]. However, only light machining tasks with certain force and torque limits can be performed by a robotic arm by considering the maximum force and torque limits of industrial robot manipulators. As per the standard procedure of any system development, the dynamic modeling of the machining process is very important to analyze and optimize the process parameters. However, simulations are commonly performed before the process, and one cannot continuously optimize the process in real time based on the feedback of real system. With the recent advancements in technology, the cyber physical system (CPS) approaches gain the popularity and show promising improvement in manufacturing process. An CPS is composed of physical object (system) and its Digital Twin (DT). The physical system is a real system while the digital twin consists of information system and data processing module. The flow of information between digital twin and its physical counterpart is regulated through a communication mechanism [7]. Digital twin already been developed to monitor, control, diagnose, and predict the different aspect in manufacturing process [8], [9], [10]. The development of accurate digital twin by incorporating the dynamic model is very important which will affect the optimization and prediction of physical manufacturing process. In this paper, the dynamic modeling for the estimation of forces and torques is considered to empower the digital model of their physical counterparts.

It is noted that sawing, nailing, milling, and drilling are performed through interaction between the machining tools and the objects being fabricated. The interaction can be modeled as continuous impulse. The quantitative measure of an impact is called impulse. For safe and effective operations, the physical characteristics of these tasks during the interaction between robot manipulator and environment should be carefully modeled for the development of DT. Two categories of impulsive motion-based machining tasks are illustrated in Fig. 1. An impulse felt at the contact point is defined as external impulse. Fig. 1(a) shows the linear impulsive motion-based tasks such as sawing, nailing, and hammering etc. Fig. 1(b) shows the linear and angular impulsive motion-based machining tasks such as rotary cutting, milling, and drilling, etc. During linear motion-based tasks, only impulsive force is required. On the contrary, both impulsive force (linear impulse) and impulsive moment (angular impulses) are required to perform linear and angular motion-based machining tasks. Compared to the linear machining tasks, rotary machining tasks are more general in the sense that they include both linear and angular motions.

With the increasing applications of automation, various research activities have been carried out to design [11] and control [12] the drilling and milling robotic mechanism for aviation [13], [14] and surgical applications [15], [16]. Also, there were many previous works related to the modeling of machining tasks [17], [18], [19], [20], [21], [22], [23], [24]. Energy-based analytical technique relying on the chip velocity and flow direction was introduced by Matsumura *et al.* [17], [18] to predict the thrust force and torque in drilling and milling operations. The chip flow direction was determined to minimize the cutting energy. This methodology was experimentally validated for a fixed drill bit. However, those methods are limited to conventional fixed drill machines for the prediction of thrust force and torque. Considering the high flexibility and intelligence, industrial robots are increasingly used in different machining tasks [22]. Industrial robots have superior kinematic performances compared with the CNC machine tools, but lower structural rigidity. The low stiffness of the robot can seriously affect the positional accuracy and machining quality in different machining tasks. Several research activities have discussed this important research issue [23], [24], [25], [26]. In those methods, authors focused on robot accuracy during drilling task by analyzing the elasto-static behavior of robot manipulators. However, to empower the DT for the prediction and optimization of the force and torque for robotic machining tasks, a more generalized analytical approach is needed including the dynamics of the robot manipulator as well as the dynamics of the chips being formed.

In regard of impulse model, various methodologies for external and internal impulses have been proposed considering the environmental model for light machining tasks [27], [28], [29]. These works, however, introduced the environmental model for linear motion-based light machining tasks only such as sawing and nailing tasks. In addition, these proposed methodologies were applied to planar cases only. The modeling of external and internal impulses for bio-inspired manipulators was introduced by Imran and Yi [30], [31]. However, they are also limited to linear impulsive motion-based applications.

In this paper, a general impulse model is proposed with application to light machining tasks, where both linear and angular impulsive motions are required. The idea is to implement the impulse model for these machining tasks. The impulse model is applicable when two bodies of known masses/inertias collide with each other (e.g., robot and object or two objects). However, the mass/inertia of the environment is unknown during machining tasks. During drilling and milling tasks, the chips are formed due to plastic deformation of the material after experiencing an impulsive force/moment over specific time interval. In this paper, analytical dynamic models (effective mass and inertia) of the environment are developed to reflect the interaction between the robot and the objects. Moreover, considering the effective mass/inertia, optimal feed rates for drilling and milling tasks are also calculated. Finally, using a 6-DOF Universal Robot (UR5e) simulation and experimental results are compared to corroborate the effectiveness of the proposed methodology.

The main contributions of this paper are as follows,

1) Provision of generalized impulse-based mathematical model for linear and angular impulse to empower the DT and its experimental validation.
2) Provision of the effective mass and effective inertia for linear and angular impulsive motion-based machining tasks.

Furthermore, the non-singular optimal workspace is calculated, and the tool direction is optimized using the belted ellipsoid analysis for the robotic drilling and milling tasks. Moreover, optimization of feed-rates considering the effective mass/inertia and task completion time for drilling and milling tasks are also provided, which are important aspects for the analysis of robotic machining operations. In a nutshell, the development of complete dynamic model and its simulation & experimental validation will empower the digital twin of light machining tasks.

The organization of the paper is as follows. In section II, the digital twin model framework is presented for robotic drilling and milling task. In section III, a closed-formed solution of linear and angular external impulses is proposed. In section IV, impulse model based belted ellipsoid is employed to analyze the feeding direction of the machining tools and optimal workspace is also analyzed to maximize the impulse exerted on the machining objects. In section V, effective mass/inertia, and optimal feed rates for two machining tasks are calculated. Experimental setup and results are described in section VI. Finally, a quantitative comparison between the experiments and simulations is made in section VII.

II. DIGITAL TWIN

Digital twin (DT) is a digital representation of the real-time operating conditions of a physical entity [32]. In this approach, every system can be a subset of two systems i.e., the real time physical system and a virtual system containing all the necessary and required information of the physical system. The simultaneous flow of information in DT allow to optimize the technology for better performance. This bi-directional dynamic relationship between physical and virtual models can improve the efficiency of product design, manufacturing/machining process, and service throughout the system's life cycle [32], [33], [34]. Digital twins successfully employed in manufacturing processes including: quality management [35], [36] to determine the quality problem and selection of better material and process, logistic planning [37] to optimize the supply chain, product development [38] by incorporating user experience, product redesign [39] by checking the compatibility of existing equipment against new design by simulating in a DT.

Three components are necessarily required to develop a digital twin (DT) for any physical object [7]. The components include: information model, communication block, and data processing module. The information model is digital model which abstract the specification of physical model to simulate its behavior for further optimization. The data processing module is responsible to manage and filter (filter out the noises) the incoming information from multiple sources including physical object to construct/mimic the live representation as much as possible. The information model and data processing module collectively form a digital twin. The communication mechanism is used to regulate the bi-directional information between digital twin and its physical counterpart by using industrial data protocols such as OPC-UA or MTConnect, etc [8]. The construction of the accurate digital model is very important in the development of efficient digital twin because it will affect the output of simulation and the analysis, control, and efficiency of the physical system.

This paper deals with the empowerment of the digital model. Fig. 2 demonstrates digital twin for light machining task including robotic milling and drilling tasks. The sensor data of physical system is being transferred to develop the digital model through communication block. In digital model, the optimization including optimal feed rates and optimal workspace based on the developed mathematical model, is being performed. And finally, the optimized information will be transferred to physical system through communication block. The detailed dynamic model for drilling and milling tasks is given in section III.

III. GENERALIZED IMPULSE MODEL FOR ROBOT MANIPULATOR

There have been previously existing impulse-based models [27], [29], which were proposed and validated for linear impulsive motion-based applications such as sawing and nailing tasks. However, for drilling and milling tasks, a general impulse model is required since these tasks involve both linear and angular impulses. It is found that a coupling effect exists between the linear and angular impulses. Coupling states that linear impulses are affected by angular velocities and vice versa. For instance, during drilling and milling machining tasks, both thrust force and torque change by changing either feed rate (linear velocity) or rotating speed (angular velocity). Considering these characteristics, a

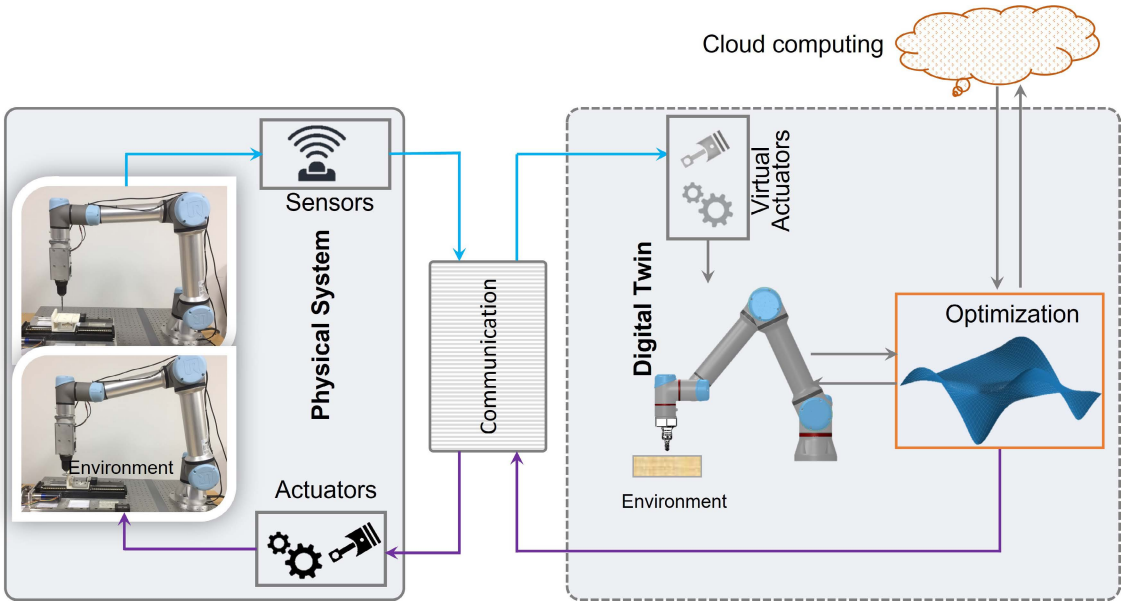

FIGURE 2. Digital Twin of robotic drilling and milling machining tasks: Bi-directional communication between physical system and virtual models.

generalized impulse model is proposed to predict the linear and angular impulses during drilling and milling tasks.

A. GENERALIZED COLLISION MODEL BETWEEN TWO RIGID BODIES

The well-known impact equation denoting the incremental change of relative linear velocities of two colliding bodies is given as [40], [41]

$$(\Delta \boldsymbol{v}_a - \Delta \boldsymbol{v}_b)^T \boldsymbol{n}_v = -(1+e)(\boldsymbol{v}_a - \boldsymbol{v}_b)^T \boldsymbol{n}_v, \tag{1}$$

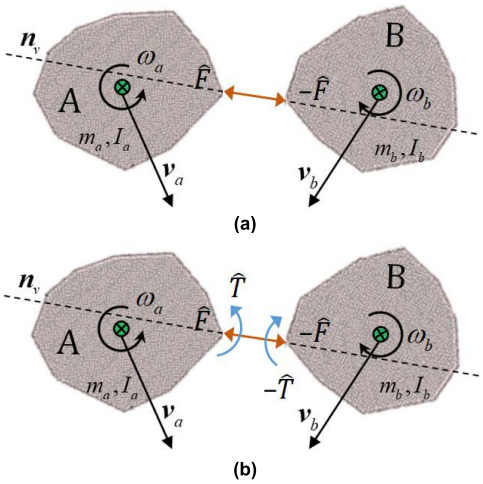

FIGURE 3. Collision model (a) Collision model including impulsive force only (b) Collision model including both impulsive force and impulsive moment.

where $\boldsymbol{v}_a$ and $\boldsymbol{v}_b$ denotes the absolute linear velocities before impact. $\Delta \boldsymbol{v}_a$ and $\Delta \boldsymbol{v}_b$ denote the linear velocity increments immediately after impact of body a and b, respectively. The coefficient of restitution e ranges from 0 to 1 for perfectively inelastic to elastic collision, and $\boldsymbol{n}_v$ denotes the unit vector along the direction of central impact as shown in Fig. 3(a). If the coefficient of restitution e is known, the relative velocity after the impact of colliding bodies can be obtained from (1). In certain applications, with existence of a moment during collision as shown in Fig. 3(b), the angular velocities could also be constrained. A moment could lead to an energy loss if it has an inelastic behavior [41]. Accordingly, a moment coefficient e_m can be introduced with properties analogous to the classical (normal) coefficient of restitution e. The moment coefficient possesses properties that control the rotational kinematics and influence the energy loss of the collision. Like (1), the incremental change in relative angular velocities can be written as follows [41]

$$(\Delta \boldsymbol{\omega}_a - \Delta \boldsymbol{\omega}_b)^T \boldsymbol{n}_\omega = -(1+e_m)(\boldsymbol{\omega}_a - \boldsymbol{\omega}_b)^T \boldsymbol{n}_\omega. \tag{2}$$

where $\boldsymbol{\omega}_a$ and $\boldsymbol{\omega}_b$ denote the absolute angular velocities before impact. $\Delta \boldsymbol{\omega}_a$ and $\Delta \boldsymbol{\omega}_b$ denote angular velocity increments immediately after impact of body a and b, respectively. $\boldsymbol{n}_\omega$ denotes the unit vector normal to the direction of central impact and the moment coefficient $e_m = 0$ corresponds to perfectly inelastic angular impact, independent of the normal coefficient e. $e_m = 1$ corresponds to perfectly elastic collision.

The eqs. (1) and (2) can be written in a combined form as follows

$$\begin{bmatrix} \boldsymbol{n}_v^T & 0 \\ 0 & \boldsymbol{n}_w^T \end{bmatrix} \begin{bmatrix} \Delta \boldsymbol{v}_a - \Delta \boldsymbol{v}_b \\ \Delta \boldsymbol{\omega}_a - \Delta \boldsymbol{\omega}_b \end{bmatrix} = -\begin{bmatrix} \boldsymbol{n}_v^T & 0 \\ 0 & \boldsymbol{n}_w^T \end{bmatrix} \begin{bmatrix} (1+e)(\boldsymbol{v}_a - \boldsymbol{v}_b) \\ (1+e_m)(\boldsymbol{\omega}_a - \boldsymbol{\omega}_b) \end{bmatrix}. \tag{3}$$

The model given in (3) is a generalized impulse model which is applicable for drilling and milling task. In the following

sub-sections, considering the body a as manipulator and the body b as the environment, the contact point velocity increment relationships for robotic arm and environment (drilling and milling operation) will be established and substituted into (3) in order to find the closed-form solution of linear and angular impulses.

B. INVERSE DYNAMIC MODEL FOR ROBOT MANIPULATOR

The generalized inverse dynamic model of the robot manipulator with respect to independent joint set ($\boldsymbol{\varphi}_a$) is given as follows [29]

$$\boldsymbol{T_a} = [I_{aa}]\,\ddot{\boldsymbol{\varphi}}_a + \dot{\boldsymbol{\varphi}}_a^T\,[P_{aaa}]\,\dot{\boldsymbol{\varphi}}_a + \boldsymbol{g_a} - \left[G_a^I\right]^T \left(\boldsymbol{F}_{ext}\ \boldsymbol{T}_{ext}\right)^T, \tag{4}$$

where $[I_{aa}]$ and $[P_{aaa}]$ denote the inertia matrix and inertial power array with respect to independent joint set, respectively. $\left[G_a^I\right]$ is Jacobian matrix that relates the velocity vector $\begin{pmatrix}\Delta \boldsymbol{v}_I \\ \Delta \boldsymbol{\omega}_I\end{pmatrix}$ at the contact point and the joint velocity vector ($\dot{\boldsymbol{\varphi}}_a$) at the independent joints. $\boldsymbol{T}_a$ and $\boldsymbol{g_a}$ stand for the joint torque and the gravity load vectors, respectively. $\boldsymbol{F}_{ext}$ and $\boldsymbol{T}_{ext}$ denote the externally applied force and moment vectors, respectively. Integration of (4) over a very short contact time will yield [29]

$$\Delta\dot{\boldsymbol{\varphi}}_a = [I_{aa}]^{-1}\left[G_a^I\right]^T \left(\hat{\boldsymbol{F}_{ext}}\ \hat{\boldsymbol{T}_{ext}}\right)^T, \tag{5}$$

where $\hat{\boldsymbol{F}}_{ext} = \int_{t_o}^{t_o+\Delta t} \boldsymbol{F}_{ext}dt$ and $\hat{\boldsymbol{T}}_{ext} = \int_{t_o}^{t_o+\Delta t} \boldsymbol{T}_{ext}dt$ denote the linear and angular external impulses, respectively. Since the position remains unchanged and velocities are finite during the impact, consequently the term involving integral $\dot{\boldsymbol{\varphi}}_a^T\,[P_{aaa}]\,\dot{\boldsymbol{\varphi}}_a$ will be zero as $\Delta t \to 0$. Similarly, the terms involving actuation torque $\boldsymbol{T_a}$ and gravity tends to zero. The kinematic relationship between the joint velocity increments and the contact point velocity increments is established as follows

$$\begin{bmatrix}\Delta \boldsymbol{v}_I \\ \Delta \boldsymbol{\omega}_I\end{bmatrix} = \left[G_a^I\right]\Delta\dot{\boldsymbol{\varphi}}_a. \tag{6}$$

Finally, for robot manipulator, by substituting (5) into (6), the linear and angular velocity increments at contact point in terms of linear and angular external impulses can be written as follows

$$\begin{bmatrix}\Delta \boldsymbol{v}_I \\ \Delta \boldsymbol{\omega}_I\end{bmatrix} = \left[G_a^I\right][I_{aa}]^{-1}\left[G_a^I\right]^T \begin{bmatrix}\hat{\boldsymbol{F}}_{ext} \\ \hat{\boldsymbol{T}}_{ext}\end{bmatrix}. \tag{7}$$

This expression can be symbolically written as

$$\begin{bmatrix}\Delta \boldsymbol{v}_I \\ \Delta \boldsymbol{\omega}_I\end{bmatrix} = \begin{bmatrix}\boldsymbol{U} & \boldsymbol{V} \\ \boldsymbol{V}^T & \boldsymbol{W}\end{bmatrix}\begin{bmatrix}\hat{\boldsymbol{F}}_{ext} \\ \hat{\boldsymbol{T}}_{ext}\end{bmatrix}, \tag{8}$$

where the coefficient matrix on right hand side is symmetric. This coefficient matrix depends on kinematic/dynamic parameters and configurations of the manipulator. Eq. (8) also explains the phenomenon of the coupling between angular/linear impulses for the case of robot manipulator.

C. DYNAMIC MODELING OF THE ENVIRONMENT

The inertial properties of the robot manipulator and the environment should be known for the implementation of the generalized impulse model to predict the linear and angular impulses. The inertia of robot manipulator $[I_{aa}]$ is known. However, the mass and inertial properties of the environment during drilling and milling task are unknown. Accordingly, in order to implement the generalized impulse-based approach, this paper introduces a methodology to calculate the effective mass and effective inertia $\left[I^*_{mcc}\right]$ for the drilling and milling tasks. The experimental calculation of effective mass and effective inertia is given in section V. In this section, the contact point velocity increment relationship is established for the environment similar to contact point velocity increment relationship of robot manipulator as given in eq. (7).

For linear impulsive motion-based machining tasks, the concept of effective mass was initially introduced by Lee *et al.* [29]. However, it was limited for linear impulse-based applications. During milling and drilling tasks, chips are formed due to plastic deformation of the material. Since each chip is formed by experiencing a certain linear and angular impulsive forces for a specific interval of time Δt_c, accordingly, both effective mass and effective moment of inertia should be defined. The effective mass/inertia is associated with the dynamics of the environment such as hardness of the material and process parameters of the machining tasks. Process parameters include feed rate, tool diameter, speed, etc.

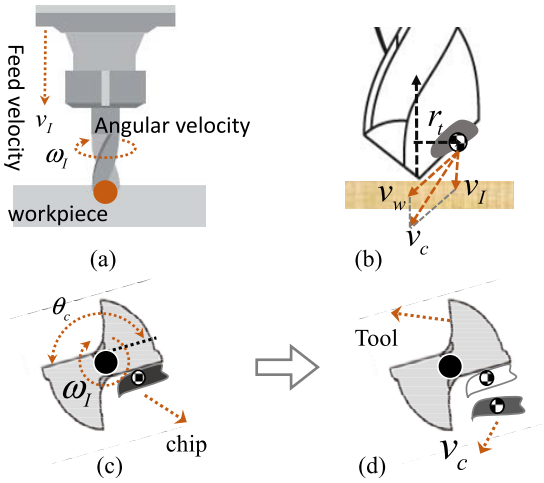

FIGURE 4. The environmental model of drilling task (a) Task description (b) Tool velocity at contact point, where ${}^c v_w = {}^c\omega_I \times r_t$, (c) Chip formation (d) Resultant velocity of the chip.

The environmental model of chip is shown in Fig. 4 and Fig. 5 for drilling and milling tasks, respectively. Note that the action and reaction exist between the robot tool and the environment. Thus, the force and moment exerted on the environment by the tool is defined as $\boldsymbol{F}_c = -\boldsymbol{F}_{ext}$ and $\boldsymbol{T}_c = -\boldsymbol{T}_{ext}$, respectively.

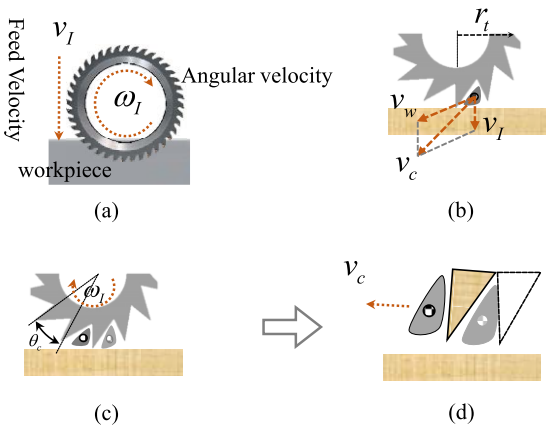

FIGURE 5. The environmental model of milling (rotary cutting) task (a) Task description (b) Tool velocity at contact point (c) Chip formation. (n: number of teeth) (d) Resultant velocity of the chip.

The linear impulsive force experienced by each chip before fracture can be written as follows

$$^{c}\boldsymbol{F}_c = \left[M_c^*\right] \frac{\Delta^c \boldsymbol{v}_c}{\Delta t_c}, \tag{9}$$

where $\Delta^c \boldsymbol{v}_c$ is the linear velocity increment of the chip due to linear impulsive force, $\left[M_c^*\right]$ is the effective mass, and $^{c}\boldsymbol{F}_c$ is the linear impulsive force vector exerted on the chip over time interval of Δt_c, which is expressed with respect to the tool frame.

As shown in Figs. 3(b) and 4(b), the velocity of the chip can be written as [42]

$$^{c}\boldsymbol{v}_c = {}^{c}\boldsymbol{v}_I + {}^{c}\boldsymbol{\omega}_I \times \boldsymbol{r}_t, \tag{10}$$

where $^{c}\boldsymbol{v}_I$ is the velocity of the manipulator to the direction normal to the workpiece, $^{c}\boldsymbol{\omega}_I$ is the angular velocity of the tool, and $\boldsymbol{r}_t$ is the vector directing from the tool center to the chip mass center. The time period can be defined as

$$\Delta t_c = \frac{d_I}{|\Delta^c \boldsymbol{v}_c|}, \tag{11}$$

where d_I denotes the width of each chip which can be defined as

$$d_I = \frac{2\pi\sqrt{\left(|\boldsymbol{r_c}|^2 + l^2\right)}}{n}, \tag{12}$$

where $\boldsymbol{r_c} = \boldsymbol{r_t}$ for drilling case as shown in Fig. 6 (c) and for milling $\boldsymbol{r_c} = \boldsymbol{r_t} - \boldsymbol{r_o}$ as shown in Fig. 6 (a). The physical representation of lead distance during milling and drilling tasks is illustrated in Fig. 6 (b) and 6 (c), respectively. The n in (12) represents the number of teeth of the tool and l represents the lead distance which is given as follows

$$l = \frac{^{c}\boldsymbol{v}_I}{|\Delta^c \boldsymbol{\omega}_c|}. \tag{13}$$

Similarly, the chip experiences impulsive moment $^{c}\boldsymbol{T}_c$, which is expressed with respect to the tool frame. The relationship

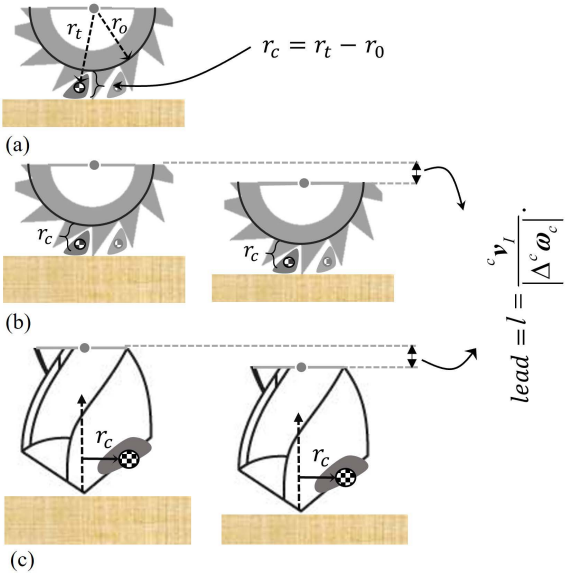

FIGURE 6. Physical representation of lead and chip radius to calculate the width of each chip. (a) Radius of chip during milling task (b) Lead distance during milling task (c) Lead distance during drilling task.

for impulsive moment in terms of effective inertia is established as follows

$$^{c}\boldsymbol{T}_c = I_{cc}\Delta\boldsymbol{\alpha} = [I_{cc}^*]\frac{\Delta^c \boldsymbol{\omega}_c}{\Delta t_c}, \tag{14}$$

where $[I_{cc}^*]$ is the effective inertia. $\Delta^c \boldsymbol{\omega}_c$ is angular velocity increment of the chip in the tool frame. Δt_c is the time period for which the chip experiences impulsive moment before fracture. That period can also be defined as follows

$$\Delta t_c = \frac{\theta_c}{|\Delta^c \boldsymbol{\omega}_c|}. \tag{15}$$

The time in both eqs. (11) and (15) will be the same. θ_c is the angle between two consecutive teeth of the tool. The initial linear/angular velocities of the chip are zero. During the formation of the chip after collision, instantaneously, the velocity increment of the chip will be the same as the velocity of the tool. If the linear and angular impulsive forces and linear and angular velocities are measurable, the effective mass and effective inertia can be calculated by using eqs. (9) to (15).

Furthermore, the relationship between velocity increments of the chip and the experienced linear and angular impulses can be established from eqs. (9) and (14) as follows

$$\Delta^c \boldsymbol{v}_c = \left[M_c^*\right]^{-1} \left({}^{c}\hat{\boldsymbol{F}}_c\right) \tag{16}$$

and

$$\Delta^c \boldsymbol{\omega}_c = \left[I_{cc}^*\right]^{-1} \left({}^{c}\hat{\boldsymbol{T}}_c\right), \tag{17}$$

where $^{c}\hat{\boldsymbol{F}}_c = {}^{c}\boldsymbol{F}_c \Delta t_c$ and $^{c}\hat{\boldsymbol{T}}_c = {}^{c}\boldsymbol{T}_c \Delta t_c$. The linear velocity increment of the chip in the global reference frame is represented as follows

$$\Delta \boldsymbol{v}_c = \left[G_c^v\right] \Delta^c \boldsymbol{v}_c = \left[G_c^v\right] \left[M_c^*\right]^{-1} \left[G_c^v\right]^T \hat{\boldsymbol{F}}_c. \tag{18}$$

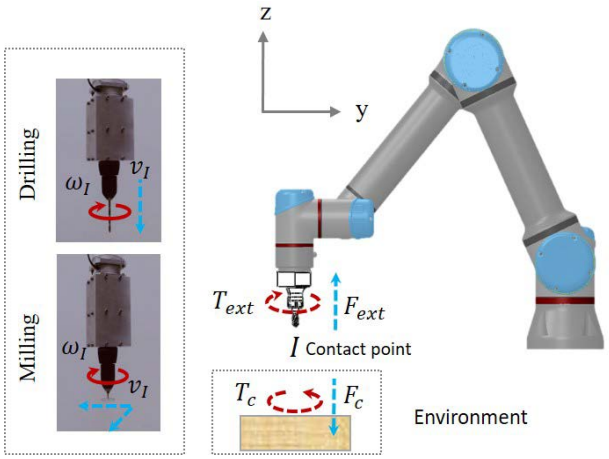

FIGURE 7. Environment model of linear and angular impulses experienced by the robot manipulator and the velocity direction during drilling and milling tasks.

Similarly, the angular velocity increment in the global reference of frame can be written as follows

$$\Delta\boldsymbol{\omega}_c = \left[G_c^{\omega}\right]\Delta^c\boldsymbol{\omega}_c = \left[G_c^{\omega}\right]\left[I_{cc}^*\right]^{-1}\left[G_c^{\omega}\right]^T\left(\hat{\boldsymbol{T}}_c\right). \quad (19)$$

The linear/angular velocity increments are written in a combined-form as follows

$$\begin{bmatrix}\Delta\boldsymbol{v}_c\\ \Delta\boldsymbol{\omega}_c\end{bmatrix} = \left[G_c^I\right]\left[I_{mcc}^*\right]^{-1}\left[G_c^I\right]^T\begin{pmatrix}-\hat{\boldsymbol{F}}_{ext}\\ -\hat{\boldsymbol{T}}_{ext}\end{pmatrix}, \quad (20)$$

where $[I_{mcc}^*] = \begin{bmatrix}[M_c^*] & 0\\ 0 & [I_{cc}^*]\end{bmatrix}$ and $[G_c^I] = \begin{bmatrix}G_c^v & 0\\ 0 & G_c^w\end{bmatrix}$.

D. EXTERNAL IMPULSES MODEL FOR ROBOT MANIPULATOR

For a robot manipulator, the relationship between incremental change in contact velocities and linear/angular external impulses is established in (7) and for environment, established in (20). If the body 'a' is considered as manipulator and the body 'b' as the environment then the substitution of (7) and (20) into (3) will yield (21), as shown at the bottom of the page, where $[n_e] = \begin{bmatrix}\boldsymbol{n}_v^T & 0\\ 0 & \boldsymbol{n}_\omega^T\end{bmatrix}$. The linear impulse acting along the normal vector $\boldsymbol{n_v}$ can be expressed as $\hat{\boldsymbol{F}}_{ext} = \hat{F}_{ext}\boldsymbol{n}_v = \boldsymbol{n}_v\hat{F}_{ext}$, and similarly, the angular impulse acting about the unit vector $\boldsymbol{n_w}$ can be expressed as $\hat{\boldsymbol{T}}_{ext} = \hat{T}_{ext}\boldsymbol{n}_w = \boldsymbol{n}_w\hat{T}_{ext}$. One can write the linear and angular impulse in a combined-form as follows

$$\begin{bmatrix}\hat{\boldsymbol{F}}_{ext}\\ \hat{\boldsymbol{T}}_{ext}\end{bmatrix} = [n_e]^T\begin{bmatrix}\hat{\boldsymbol{F}}_{ext}\\ \hat{\boldsymbol{T}}_{ext}\end{bmatrix}. \quad (22)$$

During drilling and milling machining tasks, the initial linear and angular velocities of the chips are $v_c = \omega_c = 0$. Due to plastic deformation of the material, e_m and e are zero. Finally, the closed-form solution of the linear and angular impulses is found by substituting (22) into (21) as follows (23), shown at the bottom of the page, where the first term in the denominator shows the dynamic contribution of manipulator, while the second term is associated with dynamics of the environment. The developed model in (23) can be applied to any linear and angular impulsive motion-based machining task. During the drilling and milling task, the first term in the denominator would remain the same, however, vector $[n_e]$ which determine the direction of required linear and angular impulses and the second term in the denominator would be different. Accordingly, the calculated impulses for drilling and milling tasks would be different. Fig. 7 shows the impulsive forces and impulsive moments experienced by the robot during drilling and milling tasks. The value of $[I_{mcc}^*]$ will be higher for hard materials. Accordingly, the required linear and angular external impulses will be higher for hard materials.

The moment should always be present during all collisions for the proposed model, which makes it restrictive. However, if the moment does not exist during collision, then only impulsive force with equal magnitude in opposite direction will exist and the impulse model will be simplified as given in the existing literature [29].

IV. SIMULATIONS

In this section, two different simulation analysis are performed. Firstly, the belted ellipsoid for linear and angular impulses are generated which shows the ability of a manipulator to generate impulses in/about every direction at a specific configuration for a given linear (feed rate) and angular (rpm) velocities. This analysis is important in order to choose the tool direction for a specific task. Secondly, simulations are carried out to optimize the workspace for a specific task. Further details are given in the following sub-section A and B, respectively. The simulations are performed by considering the fixed environment (infinite inertia of the environment).

$$[n_e]\left\{\left[G_a^I\right]\left[I_{aa}\right]^{-1}\left[G_a^I\right]^T + \left[G_c^I\right]\left[I_{mcc}^*\right]^{-1}\left[G_c^I\right]^T\right\}\begin{bmatrix}\hat{F}_{ext}\\ \hat{T}_{ext}\end{bmatrix} = -[n_e]\begin{bmatrix}(1+e)(v_I - v_c)\\ (1+e_m)(\boldsymbol{\omega}_I - \boldsymbol{\omega}_c)\end{bmatrix}, \quad (21)$$

$$\begin{bmatrix}\hat{F}_{ext}\\ \hat{T}_{ext}\end{bmatrix} = \frac{-[n_e]\begin{bmatrix}v_I & \boldsymbol{\omega}_I\end{bmatrix}^T}{[n_e]\left\{\left[G_a^I\right]\left[I_{aa}\right]^{-1}\left[G_a^I\right]^T + \left[G_c^I\right]\left[I_{mcc}^*\right]^{-1}\left[G_c^I\right]^T\right\}[n_e]^T}, \quad (23)$$

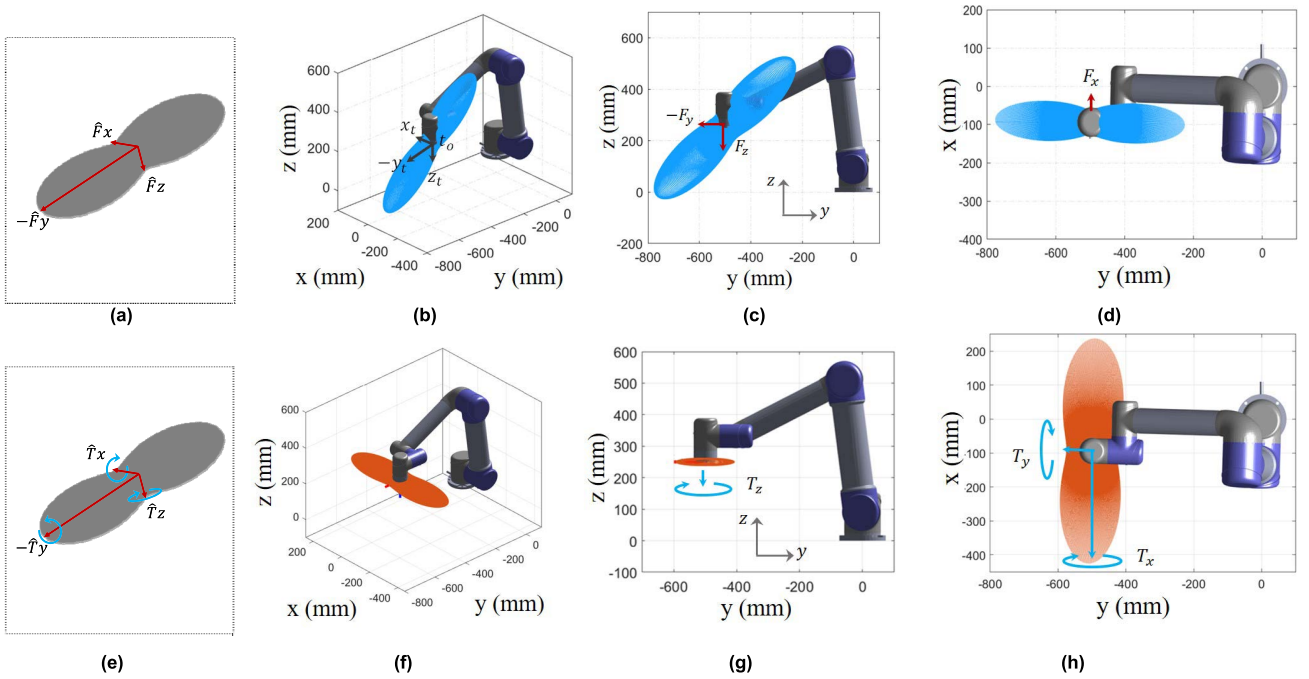

FIGURE 8. Impact geometry (a) General belted ellipsoid for linear impulse. (b-d) Belted ellipsoids of linear impulse for UR5e robotics arm in different views: t_O denotes the origin of tool frame. (e) General belted ellipsoid for angular impulse (f-h) Belted ellipsoids of angular impulse for UR5e robotics arm in different views. Linear velocity = 0.05m/sec and Angular velocity 20rad/sec.

The values of e_m and e will be zero due to plastic deformation of the material during drilling and milling tasks.

A. PERFORMANCE ANALYSIS IN TERMS OF BELTED ELLIPSOID

In this sub-section, the performance of robotic machining tasks is analyzed in terms of normalized impact geometry. Walker [43] defined the dynamic impact ellipsoid as $u^T[G_a^I][I_{aa}]^{-2}[G_a^I]^T u \leq 1$, where the column of u represents the principal axes of the dynamic impact ellipsoid. However, there are two limitations in those ellipsoids [44]. Firstly, the magnitude and direction of task velocity are not considered which play an important role in the magnitude of impulsive force. And, secondly, the magnitude of those ellipsoid does not directly represent the impact force. To overcome these issues, Kim *et al.* [44] introduced the dynamic and generalized impact geometry which is given as $n^T\left[G_a^I\right][I_{aa}]^{-1}\left[G_a^I\right]^T n\hat{F}_{ext} \leq 1$, where n is the unit vector normal to the plan of collision impact. The current study extends the latter concept to construct the linear and angular impulse belted ellipsoids. The concepts of belted ellipsoids for linear and angular impulses are illustrated in Fig. 8(a) and (e), respectively. The distance from the center to the surface of each ellipsoid shows the amount of linear/angular impulse along/about each direction for a given contact point velocity. So, the longer the distance, the greater linear or angular impulse can be applied to that direction.

In the given setup, a separate motor is used in drill assembly to rotate the tool at specific RPM. In machining operations, the required torque is applied by drill assembly's motor while the feed rate is provided by the robotic arm. In other words, the robotic arm applies the linear velocity only.

The linear impulses should be maximized in a specific direction to perform the machining task by controlling the linear velocity of the robotic arm. Since the linear and angular impulses are coupled as described in eq. (23), the manipulator experiences the angular impulse as a reaction; accordingly, the angular impulses should be minimized in the direction of performing a machining task. Furthermore, the externally applied impulses may damage the robotic arm's link and joints. So, the material selection and stress analysis during the manipulator design are also very important. Since an already developed commercial robotic arm is used in this study; accordingly, the detail structure's stress analysis is not discussed.

The external impulses can be maximized or minimized for kinematic redundant manipulators by using different algorithms [44], [45]. For the given UR5e non-redundant robot, the tool direction is decided based on the impulse geometry to maximize the linear impulse and minimize the angular impulses.

Assuming the 0.05m/sec linear and 20rad/sec angular velocities at contact point in/about every direction, respectively; the belted ellipsoids for linear and angular impulses are constructed based on impulse models of (23). The linear and angular belted ellipsoids are shown in Fig. 8 (b-d) and (f-h) in different views, respectively. Since the angular impulses are minimum about the z-axis; accordingly, the drilling and milling operation are performed about z-axis to minimize the coupling effect. Though the x-axis or y-axis

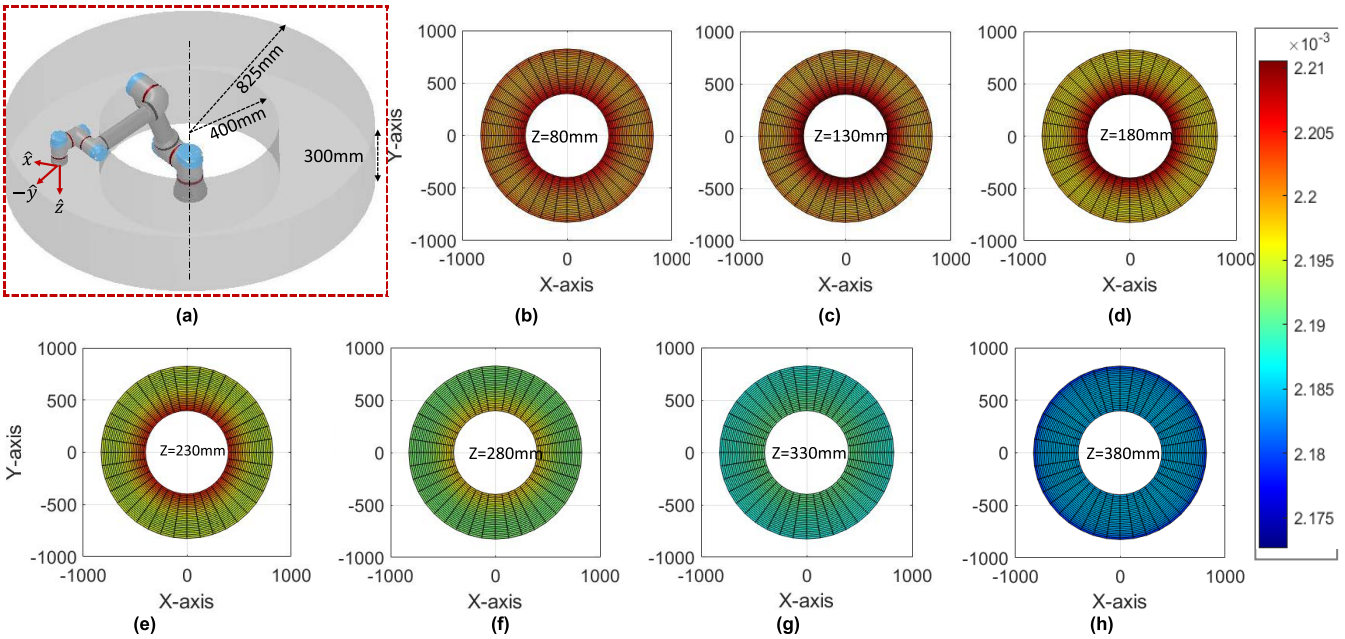

FIGURE 9. Drilling case: Impulse analysis in selected workspace with (radius in XY plane: 400 to 825mm) at different z-axis values: Considering that the linear impulse is along z-axis. (a) Specified workspace (b) linear impulse at z=80mm (c) linear impulse at z=130mm (d) linear impulse at z=180mm (e) linear impulse at z=230mm (f) linear impulse at z=280mm (g) linear impulse at z=330mm (h) linear impulse at z=380mm. Color bar denotes the linear impulse variation in Ns. Feed rate: 1mm/sec, RPM: 1200.

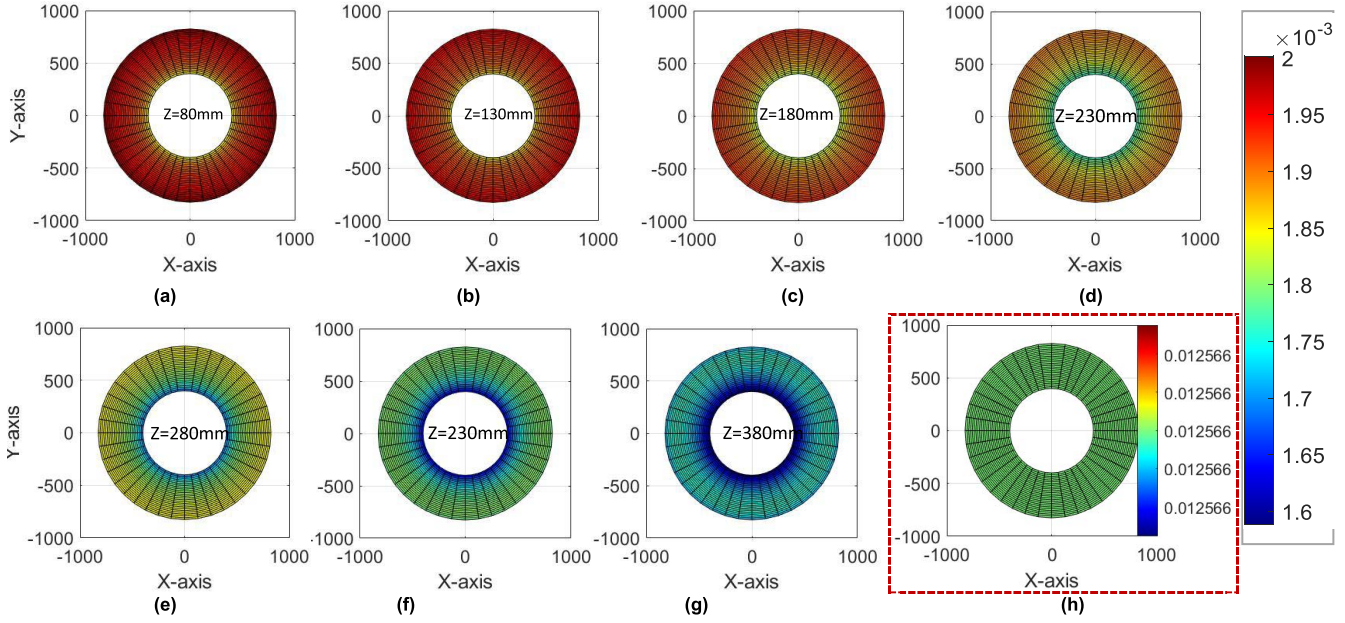

FIGURE 10. Milling case: Impulse analysis for the same workspace: Considering that the linear impulse is along -y-axis. (a) linear impulse at z=80mm (b) linear impulse at z=130mm (c) linear impulse at z=180mm (d) linear impulse at z=230mm (e) linear impulse at z=280mm (f) linear impulse at z=330mm (g) linear impulse at z=380mm (h) Angular impulse. Color bars denotes the linear impulse variation in Ns and angular impulse in Nms. Feed rate: 1mm/sec, RPM: 1200.

can be considered as the direction of the feed velocity for the milling task, the y-direction is recommended since the linear impulse is maximum along that direction as shown in Fig. 8 (c, d). Since the tool rotation is recommended about z-axis, accordingly, the feed velocity will be provided along z-axis for drilling task. The recommended tool directions will help to minimize the angular impulse and maximize the linear impulses.

B. OPTIMIZATION OF WORKSPACE

For redundant manipulators, kinematic redundancy can be utilized to maximize the linear impulses and minimize the angular impulses [44], [45]. However, one can still find optimal workspace that assures maximum performance in terms of the linear impulse/angular impulses. It is also important to choose the non-singular workspace as the impulses would be very large at singular configurations [43].

The non-singular workspace is considered with radius of 400mm to 825 mm in xy-plane and displacement along the z-axis from 80mm to 380 mm as shown in Fig. 9 (a) which is calculated based on the manipulability measure index ($w = |\det[G_a^I]|$) [43]. Then, the optimized workspace volume is calculated where the linear impulses are maximum and angular impulses are minimum. It is considered that the tool is always perpendicular to the horizontal (xy-plane) and tasks are being performed at 1200 rpm with 1mm/sec feed rate. Firstly, the linear impulses are calculated for drilling task by considering the direction of linear impulse along and about z-axis of tool frame. The calculated linear impulses in xy-plane at different values of z-axis are shown in Fig. 9 (b-h). Since the orientation of tool is fixed for this analysis; accordingly, the angular impulses are not changing much in whole workspace. In overall workspace, the variation in linear impulse is very small for drilling task as can be seen from color bar in Fig. 9. Accordingly, it is recommended that the whole non-singular workspace can be used for drilling operation.

Next, the linear impulses are calculated for milling task by considering the directions of linear and angular velocities along and about y-axis and z-axis, respectively. The calculated linear impulse in xy-plane at different values of z-axis are shown in Fig. 10(a-g). The variation in linear impulse is considerable. In order to perform the task with maximum linear impulses along the y-direction, the workspace with z-axis less than 200mm (near to ground) is recommended based on the observation of Fig. 10. The orientation of tool and direction of linear and angular velocity could be other than used directions. For those cases, the analysis can be performed in the same manner.

V. EFFECTIVE MASS/EFFECTIVE INERTIA CALCULATION

In this section, the effective mass and effective inertia are calculated experimentally for both machining operations. While calculating the effective mass/inertia, the inertia of the robot/machine should be infinite in order to apply the equation (9) and (14). Accordingly, the robotic arm was fixed, and the feed-rate was provided by using a separate mechanism. The effective mass and inertia can also be calculated by using a fixed drilling machine. For the validation of effective mass/inertia, the feed rate will be provided by using a robot to include dynamics of robot (section VI).

The effective mass depends on three parameters (F_c; the force required to form a chip, Δt_c; the time required to form a chip, and $\Delta^c v_c$; the velocity increment of the chip). Moreover, the Δt_c depends upon diameter and number of the teeth of the tool. However, the diameters of the tool cannot be optimized as it is the requirement of any specific task. Furthermore, the hard material required more impulsive force F_c, accordingly, the value of the effective mass will be higher. Similar is the case for effective inertia. The trend of affective mass against different material has already been presented and evaluated by Imran *et al.* [28]. Considering those reasons, the effect of diameter of tool and hardness of material are not discussed

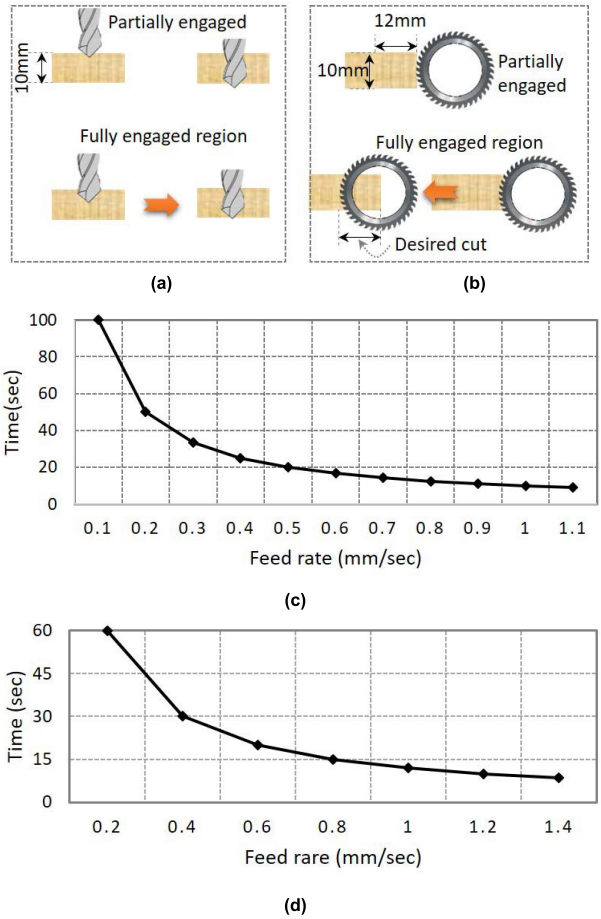

FIGURE 11. Task objective and tool engagement during drilling and milling tasks (a) Drilling task (objective: to drill through a plate of 10mm thick of ABS material) (b) Milling task (objective: to cut a plate of 10mm width and 12mm thick of ABS material. (c) Time required to complete drilling task at different feed rate (d) Time required to complete milling task at different feed rates.

in this paper. In order to optimize the process parameters, the effective mass and inertia are calculated at different feed rates and RPMs for drilling and milling tasks. The same material (ABS) is used for drilling and milling operations.

It is found that the effective mass/inertia is different for milling and drilling tasks even if the tasks are performed at the same feed rate with the same speed. This is because the required force/torque and contact time ($\Delta t_c = \frac{\theta_c}{|\Delta^c \omega_c|}$) are different due to different geometry (number of teeth) of tools. During drilling and milling operations, elaboration of engagement of the tool with material are shown in Fig. 11(a) and (b), respectively. At start and at the end, the tool is partially engaged. The effective mass and effective inertia are calculated during the fully engaged period of the tool with the material. During drilling operation, the task is to make a hole through 10mm thickness ABS material plate as shown in Fig. 11(a). During milling task, the task is to cut a plate of 10mm wide and 12mm thick of ABS material as shown in Fig. 11(b). The time required to complete the task during drilling and milling tasks at different feed rates was measured

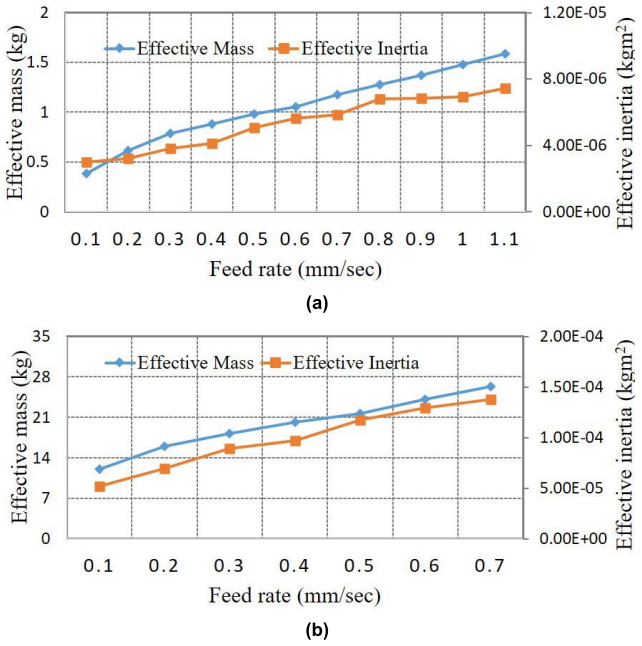

FIGURE 12. Effective mass and effective inertia during drilling task at different feed rates (a) At 1200rpm (b) At 370rpm.

through experiment as shown in Fig. 11(c) and (d). The time is exponentially decreased as the feed rate is increased.

A. DRILLING TASK

Drilling task is performed at two different speeds (rpms) with different feed rates. The diameter of the tool is 5.5 mm. The effective mass and effective inertia are calculated by using eqs. (9) and (14), where the force and torque data are measured by a FT sensor. Since the chips are being formed due to plastic deformation of the parts; accordingly, the angular velocity of the chip will be the same as the tool and linear velocity is calculated by using (10). Contact time is calculated by using eq. (13) and (15). The calculated values of effective mass/effective inertia are shown in Fig. 12(a) and 12(b) at 1200rpm and 370rpm, respectively. It is observed that the effective mass/inertia is linearly increasing with feed rates and that the values of effective mass/inertia are higher at low speed (rpm). This makes sense because

- At high speed (rpm), the time required (25ms) to form a chip is much smaller compared to the time taken (81ms) at low speed (rpm).
- Secondly, the linear velocity obtained by using (10) is also higher at high speed (rpm).

Based on (9) and (14), it is inferred that the shorter contact time and higher contact velocities tend to decrease the effective mass and effective inertia. Accordingly, the effective mass and effective inertia values are higher at low speed as shown in Fig. 12.

B. MILLING (ROTARY CUTTING) TASK

The milling operation is performed at 1200rpm with different feed rates. At low speeds, the manipulator experiences more

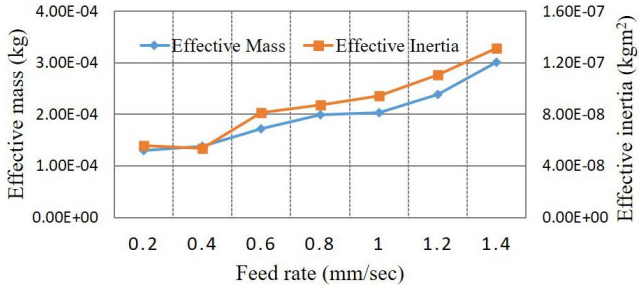

FIGURE 13. Effective mass and effective inertia during milling task at 1200rpm.

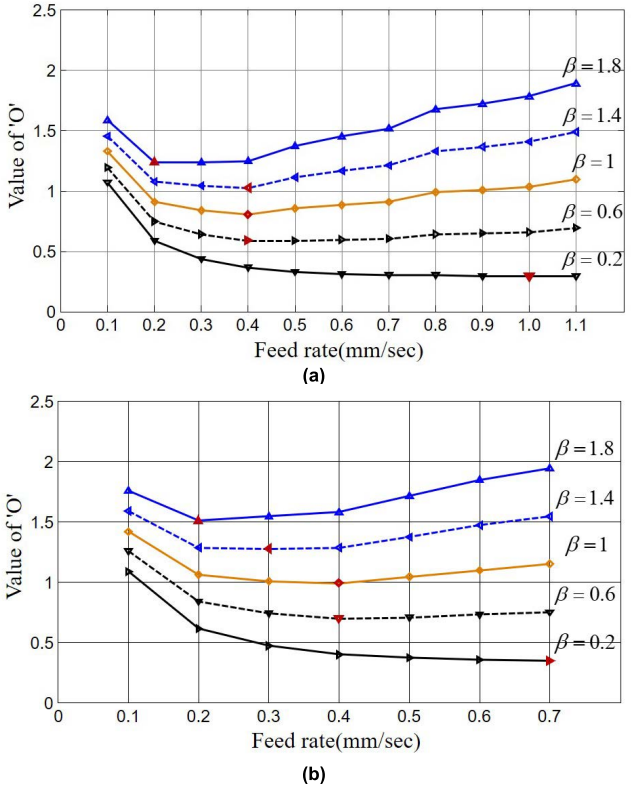

FIGURE 14. Optimization during drilling task with different values of β (a) At 1200rpm. (b) At 370rpm. The optimal feed rates are highlighted as red marker corresponding to the minimum values of objective function 'O'.

vibration due to small teeth and large diameter of the tool as compared to drilling tool. The diameter of the cutting tool is 40mm. The tool has 100 teeth; accordingly, the contact time for each chip is calculated as 0.5msec. The effective mass and inertia are calculated again by using the eqs. (9) to (14) and the values are shown in shown in Fig. 13. Due to very short contact time, the values of effective mass and effective inertia are smaller compared to drilling task, however, the trend is the same.

C. OPTIMAL FEED RATES

During drilling/milling machining tasks, too high or too low feed rates at a specific speed (rpm) can affect the quality of machining operation or damage the tool. Usually, for each material the optimal feed rate is recommended for

machining operation. However, additional measures need to be considered in robotic machining tasks since industrial robotic arms have maximum force limit that should not be exceeded for safety concern. Taguchi technique and response surface methodology are widely used to optimize the process parameters during machining process. Different optimization research activities were carried out by considering the hole quality and surface roughness for specific materials [46], [47], [48], [49]. Rao *et al.* [49] modeled and optimized the effect of cutting parameters on surface roughness and tool vibration by using response surface methodology, artificial neural network, and support vector machine for regression.

In this sub-section, an optimization technique is proposed to find the optimal feed rates considering the effective mass and effective inertia. The effective mass/inertia is more generalized property since it elaborates the dynamics of the environment. The higher value of effective mass/inertia implies that the manipulator experiences more burden. Accordingly, the objectives are defined as follows

- Minimization of the effective mass/inertia.
- Minimization of the time required to complete the machining task.

At higher feed rates, the tasks can be completed in minimum time while, the effective mass and effective inertia will increase. There exists a tradeoff between task completion time and effective mass/inertia, accordingly, a combined objective function is proposed as follows

$$\min(O) = \frac{1}{s}\sum_{i=1}^{s}\left(\frac{t_i}{t_{i_{\max}}} + \beta\frac{E_i}{E_{i_{\max}}}\right) \tag{24}$$

subject to

$$T_c \leq T_{\max} \text{ and } F_c \leq F_{\max} \tag{25}$$

The performance index is to minimize the objective function 'O', where 't_i' represents the task completion time, 'E_i' (effective mass and effective inertia) denotes the dynamics of the environment, and 's' denotes the number of environment factors. In our case, we have two environments factors; effective mass and effective inertia. $F_{\max}$ and $T_{\max}$ denote the maximum force and torque limits of the robot manipulator, respectively. F_c and T_c are the measured force and torque experienced by chip, which will be used in calculation of effective mass and effective inertia, respectively. β is the priority factor. $\beta = 1$ employs the equal contribution of both objective functions (t_i, E_i). $\beta > 1$ gives more weightage to the dynamics of environment (E_i), while $\beta < 1$ gives more weightage to task completion time (t_i).

Firstly, the optimization for drilling task is performed. The optimization results with different values of β are shown inFig. 14. The optimal feed rates, corresponding to the minimum value of the objective function 'O', are highlighted as red marker. The task completion time is minimum at high feed rates while the dynamics of the environment (effective mass/inertia) is minimum at low feed rates. Increasing β gives more priority to the dynamics of the environment; accordingly, the optimal feed rates are decreasing. Similarly, the optimization results for milling task are shown in Fig. 15. Optimal feed rates are highlighted as red marker with different values of β. The proposed optimization technique can be effectively applied to find the optimal feed rates during machining tasks. In our experiment, an equal priority ($\beta = 1$) is given to both objectives. From Figs. 14 and 15, optimal feed rates were recommended as 0.4mm/sec and 1mm/sec for drilling and milling tasks, respectively.

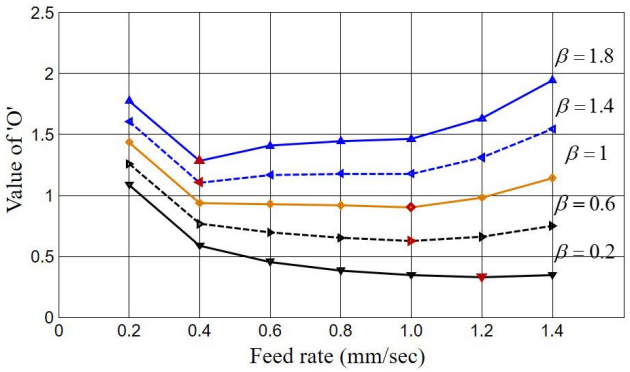

FIGURE 15. Optimization during milling (rotary cutting) task with different values of β at 1200rpm. The optimal feed rates are highlighted as red marker correspond to the minimum values of objective function 'O'.

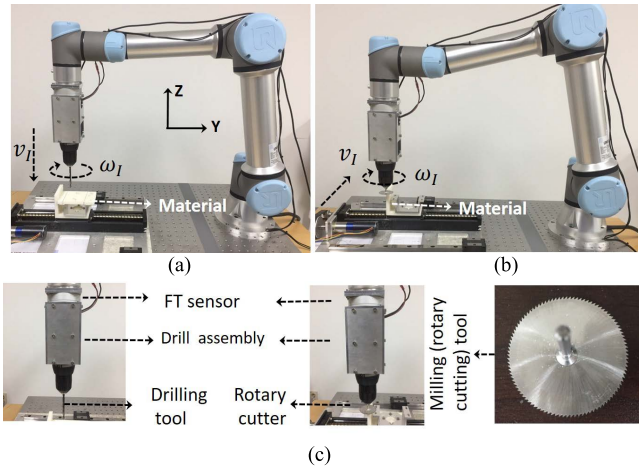

FIGURE 16. Experimental setup. (a) Drilling task (b) Milling (rotary cutting) task (c) Details of end-effectors.

VI. EXPERIMENTATION

A 6-DOF Universal Robotic arm (UR5e) is used for experimentations of drilling and milling tasks. The kinematics is used as calculated by Kebria *et al.* [50]. The dynamics of robot is calculated based on multiple cylinder method for each link, as proposed and verified by Kufieta [51]. The experimental setup is shown in Fig. 16. Figs. 16(a) and 16(b) illustrate the setup for robotic drilling and milling tasks, respectively. The drill assembly is attached at the distal end of the robot manipulator and FT (6-axis) sensor of Robotous company (RFT76-HA01) is installed between the drill assembly and the robot end-effector to measure the force and torque

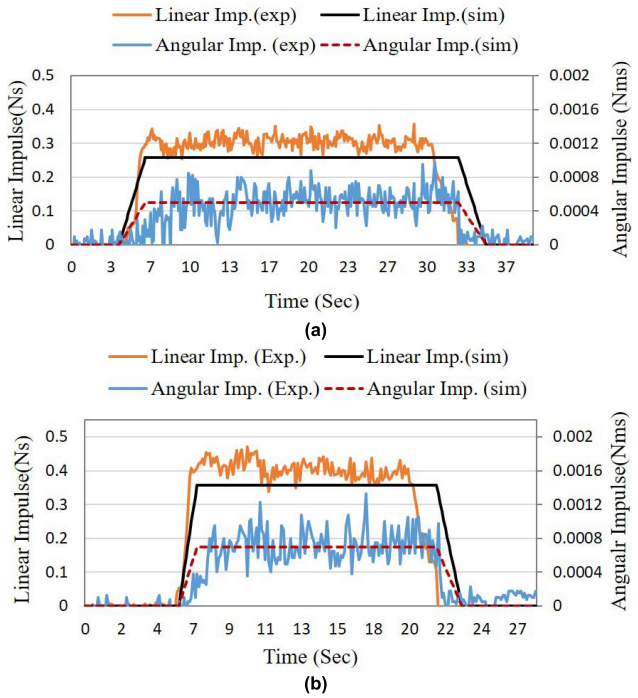

FIGURE 17. Comparison of simulation and experimental results for drilling task at 1200rpm (a) Linear and angular impulses at feed rate 0.4 mm/sec (b) Linear and angular impulses at feed rate 0.7 mm/sec.

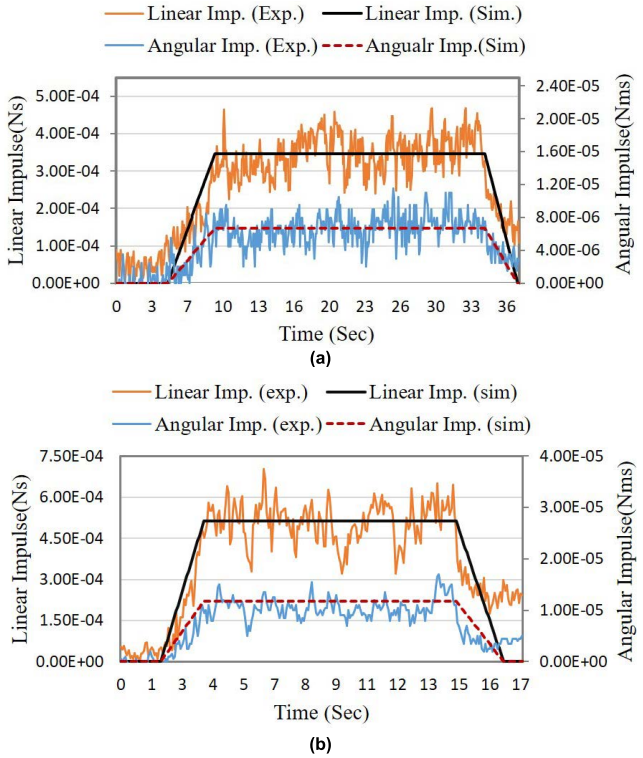

FIGURE 18. Comparison of simulation and experimental results for milling (rotary cutting) task at 1200rpm (a) Linear and angular impulses at feed rate 0.4 mm/sec (b) Linear and angular impulses at feed rate 1 mm/sec.

data as shown in Fig. 16(c). The maximum force and torque limits for the sensor are 300N and 10Nm along and about each axis, respectively. For both machining tasks, the angular velocity is about z-axis, while the feed velocity is along z-axis and x-axis of the global coordinate system for drilling and milling task, respectively.

A. DRILLING TASK

Firstly, experiments for drilling task are performed at 1200rpm with two feed rates. An ABS material of 10mm thickness is drilled. The force and torque data are measured by FT sensor. Furthermore, the linear and angular impulses are calculated by integrating the measured force and torque data over contact time, which is 25 msec. Fig. 17 shows the experimental results of linear and angular external impulses for drilling task.

Based on the proposed model of external impulse in (23), embedding the effective mass and effective inertia (second part of the denominator of (23)), simulations are performed by using MATLAB. The linear velocity at the contact point is calculated by using (10) and angular velocity is calculated as 125.66 rad/sec. The simulations are performed for fully engaged region. The slope in Fig. 17 stands for partially engaged region. The simulation and experimental results are identical as can be seen in Fig. 17.

B. MILLING TASK

Secondly, the experiments for milling task are performed at 1200rpm with two feed rates. The drill assembly is capable of performing both drilling and milling tasks. Rotary cutter of 40mm diameter is used as shown in Fig. 16(c). Same ABS material is used for milling operation. The milling (rotatory cutting) task is performed by cutting a plate of 10mm width up to 12mm thickness. To measure the linear and angular impulses, the integration of measured force and torque data is performed over 0.5msec contact time and results are shown in Fig. 18. The simulations are performed by using eq. (23) with consideration of effective mass and effective inertia as calculated in section (V). The simulation and experiment results are well identical.

VII. COMPARATIVE ANALYSIS

There are three main approaches to determine thrust forces and torque during machining operations: experimental, numerical, and analytical approaches. The major drawback of analytical approach concerns its reliability. Different research activities have been carried out to propose the analytical model to predict the thrust force and torque in drilling and milling tasks and simulation and experimental results are compared. Naisson *et al.* [20] introduced an analytical model based on modified Merchant's method. Matsumura *et al.* [17], [18] introduced an energy-based analytical technique relying on the chip velocity and flow direction to predict the thrust force and torque in drilling and milling operations. Strenkowski *et al.* [19] predicted the thrust force and torque in drilling by using a finite element technique. However, in prediction of impulsive force and torque for robotic

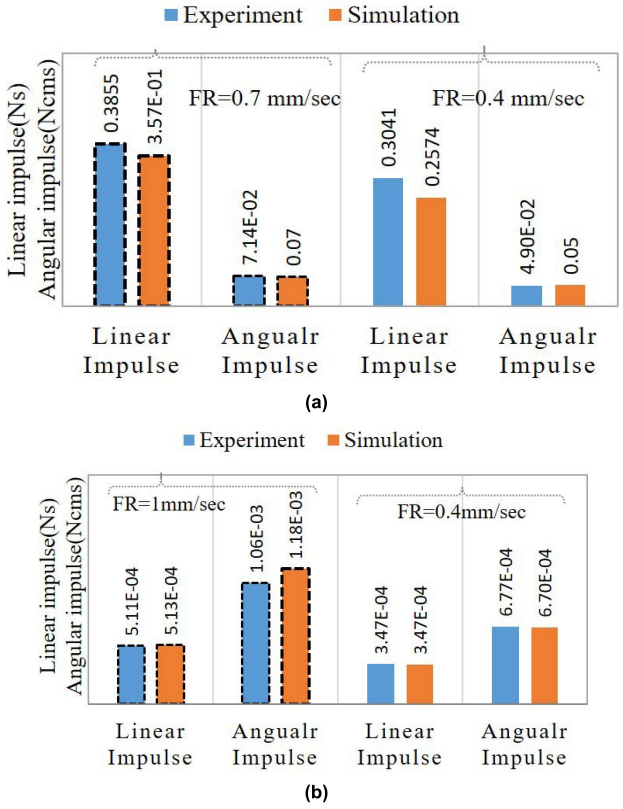

FIGURE 19. Quantitative comparison of simulation and experimental results (a) Linear and angular impulses during milling task. (b) Linear and angular impulses during drilling task. FR implies the feed rate.

machining operations, more generalized analytical approach is required to include the dynamics of the robot manipulator along with the dynamics of the chips being formed. Based on our proposed impulse-based method, the dynamics of the manipulator can be easily combined with dynamics of the environment. Furthermore, this method can be effectively applied to optimize the external impulse for kinematic redundant manipulators as applied in previous research [43], [45].

The analytical closed-form model of linear and angular impulses has been developed by integrating the dynamic model of robot manipulator. The equation (5) is formulated by integrating the dynamic model given in (4), as follows

$$\int_{t_o}^{t_o+\Delta t} \boldsymbol{T_a} dt = \int_{t_o}^{t_o+\Delta t} [I_{aa}]\ddot{\boldsymbol{\varphi}}_a dt + \int_{t_o}^{t_o+\Delta t} \dot{\boldsymbol{\varphi}}_a^T [P_{aaa}]\dot{\boldsymbol{\varphi}}_a dt + \int_{t_o}^{t_o+\Delta t} \boldsymbol{g_a} dt - \int_{t_o}^{t_o+\Delta t} \left[G_a^I\right]^T \left(\boldsymbol{F}_{ext}\ \boldsymbol{T}_{ext}\right)^T dt. \quad (26)$$

In comparison of simulation and experimental results, the contact time is very important. Usually, Δt is an infinitesimally short time interval. Therefore, the positions and orientation remain unchanged since all velocities and angular velocities remain finite. Any propagation of deformation wave and tension through bodies can be neglected since such processes require finite periods of time. Hence, all bodies of the system can be treated as rigid bodies during impact. Only impulsive forces and impulsive moments cause discontinuous changes of velocities. If the contact time is not short enough, these terms $\boldsymbol{T}_a$ and $\dot{\boldsymbol{\varphi}}_a^T [P_{aaa}] \dot{\boldsymbol{\varphi}}_a$ will not be completely zero and show some contribution and hence cause error in results.

In this section, the simulation and experimental results are compared quantitatively for milling and drilling task as shown in Figs. 19(a) and 19(b), respectively. In previous impulse-based applications, the contact time was used as 10msec [29] in comparison of simulation and experimental results. In fact, the contact time depends on the speed (rpm) and number of teeth. The contact time will be decreased by increasing the RPMs as given in (10) and (15). The detail discussion and calculated values of contact times at different RMPs was provided in section (V). In experiments, both tasks are performed at the same speed, but the contact time is still different because the number of teeth of tool during drilling (two teeth) and milling (100 teeth) are different. During milling task, contact time (i.e., 0.5msec) is very short; accordingly, the simulation and experiment results are well identical. However, in the drilling task, the contact time (25msec) is comparatively more than milling task. Hence, there exists small error (0.05 Ns) between simulation and experimental results. In conclusion, the comparison made in this section validates the proposed mathematical model for linear and angular impulses along with the mathematical model and experimental calculations of effective mass and effective inertia. The development of complete dynamic model to estimate the forces and torques and its experimental validation will certainly empower the Digital model which can be used to optimize the process parameters in real time. In order to implement the digital twin in real time for any machining process, the robotic arm needs to be equipped with joint encoders and force/torque sensor to measure the robot configuration and drilling/milling force and torque values to calculate the effective mass and effective inertia based on the proposed methodology. In the beginning of any machining process, some parameters need to feed manually by the user/operator including the diameter and no. of teeth of the tool and completion time (if any) etc. In real time, for specific material, the digital twin system receives the data through communication block at different feed rates and rpms to optimize the tool direction and feed rates. And then the Digital Twin will transfer the optimized values of the process parameters to the real system through communication block to perform the task repeatedly. Furthermore, the digital twin will continuously predict the future state to safeguard the robot manipulator. However, for different materials or different machining process, the real time parameters as mentioned above need to pass on again to the Digital Twin model.

VIII. CONCLUSION

In contrast to fixed conventional fixed drill machines, robot manipulators provide the large dexterous workspace and have ability to effectively perform different light machining tasks, as the manipulator could change the posture of a machining tool using many degrees of freedom.

The advantages of the proposed generalized impulse model are as follows.

1) Machining tasks that combine both linear and angular motions can be analyzed in terms of impulse model.
2) Each machining task can be modeled in terms of effective mass/inertia. Furthermore, the optimal feed rates could be calculated for drilling and milling tasks by considering the effective mass/effective inertia and minimum task completion time.
3) Optimal tool direction based on the belted ellipsoid analysis along with non-singular optimal workspace could be calculated for robotic drilling and milling tasks.

This study needs more improvement in effective mass/inertia. A continuum model is preferred for better accuracy. Incorporating kinematic redundancy in robot manipulator would enhance the geometry of the belted ellipsoid.

The proposed methodology can be beneficially applied to develop DT model of the of variety of linear and angular impulsive motion-based machining tasks such as burring, sawing, grinding, boring, cutting, hammering, etc.

REFERENCES

[1] T. Olsson, M. Haage, H. Kihlman, R. Johansson, K. Nilsson, A. Robertsson, M. Björkman, R. Isaksson, G. Ossbahr, and T. Brogrdh, "Cost-efficient drilling using industrial robots with high-bandwidth force feedback," *Robot. Comput.-Integr. Manuf.*, vol. 26, no. 1, pp. 24–38, Feb. 2010.

[2] L. Zhang and X. Wang, "Dynamic control of a flexible drilling robot end-effector," in *Proc. 24th Chin. Control Decis. Conf. (CCDC)*, May 2012, pp. 2199–2204.

[3] H. Lim, S.-H. Lee, B.-R. So, and B.-J. Yi, "Design of a new 6-DOF parallel mechanism with a suspended platform," *Int. J. Control, Autom. Syst.*, vol. 13, no. 4, pp. 942–950, Aug. 2015.

[4] E. Abele, M. Weigold, and S. Rothenbücher, "Modeling and identification of an industrial robot for machining applications," *CIRP Ann.-Manuf. Technol.*, vol. 56, no. 1, pp. 387–390, Mar. 2007.

[5] T. Dietz, A. Pott, and A. Verl, "Practice for planning and realization of advanced industrial robot systems," in *Proc. 44th Int. Symp. Robot. (ISR)*, Seoul, South Korea, Oct. 2013. pp. 1–4.

[6] G. Wang, H. Dong, Y. Guo, and Y. Ke, "Dynamic cutting force modeling and experimental study of industrial robotic boring," *Int. J. Adv. Manuf. Technol.*, vol. 86, nos. 1–4, pp. 179–190, Sep. 2016.

[7] Y. Lu, C. Liu, K. I.-K. Wang, H. Huang, and X. Xu, "Digital twin-driven smart manufacturing: Connotation, reference model, applications and research issues," *Robot. Comput.-Integr. Manuf.*, vol. 61, Feb. 2020, Art. no. 101837.

[8] G. Kiswanto, "Digital twin approach for tool wear monitoring of micro-milling," *Proc. CIRP*, vol. 93, pp. 1532–1537, Jan. 2020.

[9] Z. Zhu, C. Liu, and X. Xu, "Visualisation of the digital twin data in manufacturing by using augmented reality," *Proc. CIRP*, vol. 81, pp. 898–903, Jan. 2019.

[10] W. Kritzinger, M. Karner, G. Traar, J. Henjes, and W. Sihn, "Digital twin in manufacturing: A categorical literature review and classification," *IFAC-PapersOnLine*, vol. 51, no. 11, pp. 1016–1022, 2018.

[11] Z. Wang, X. Qin, J. Bai, X. Tan, and J. Li, "Design and implementation of multifunctional automatic drilling end effector," *IOP Conf. Ser., Mater. Sci. Eng.*, vol. 187, no. 1, Mar. 2017, Art. no. 012032.

[12] M. Hessinger, M. Pingsmann, J. C. Perry, R. Werthschutzky, and M. Kupnik, "Hybrid position/force control of an upper-limb exoskeleton for assisted drilling," in *Proc. IEEE/RSJ Int. Conf. Intell. Robots Syst. (IROS)*, Sep. 2017, pp. 1824–1829.

[13] F. von Drigalski, L. E. Hafi, P. M. U. Eljuri, G. A. G. Ricardez, J. Takamatsu, and T. Ogasawara, "Vibration-reducing end effector for automation of drilling tasks in aircraft manufacturing," *IEEE Robot. Autom. Lett.*, vol. 2, no. 4, pp. 2316–2321, Oct. 2017.

[14] D. Chen, P. Yuan, T. Wang, C. Ying, and H. Tang, "A compensation method based on error similarity and error correlation to enhance the position accuracy of an aviation drilling robot," *Meas. Sci. Technol.*, vol. 29, no. 8, Aug. 2018, Art. no. 085011.

[15] S. Shim, H. Choi, D. Ji, W. Kang, and J. Hong, "Robotic system for bone drilling using a rolling friction mechanism," *IEEE/ASME Trans. Mechatronics*, vol. 23, no. 5, pp. 2295–2305, Oct. 2018.

[16] Y. Dai, Y. Xue, and J. Zhang, "Vibration-based milling condition monitoring in robot-assisted spine surgery," *IEEE/ASME Trans. Mechatronics*, vol. 20, no. 6, pp. 3028–3039, Dec. 2015.

[17] T. Matsumura and J. Leopold, "Simulation of drilling process for control of burr formation," *J. Adv. Mech. Des., Syst., Manuf.*, vol. 4, no. 5, pp. 966–975, 2010.

[18] T. Matsumura and S. Tamura, "Cutting force model in milling with cutter runout," in *Proc. 16th CIRP Conf. Modeling Mach. Oper.*, vol. 58, 2017, pp. 566–571.

[19] J. S. Strenkowski, C. C. Hsieh, and A. J. Shih, "An analytical finite element technique for predicting thrust force and torque in drilling," *Int. J. Mach. Tools Manuf.*, vol. 44, nos. 12–13, pp. 1413–1421, Oct. 2004.

[20] P. Naisson, J. Rech, and H. Paris, "Analytical modeling of thrust force and torque in drilling," *Proc. Inst. Mech. Eng., B, J. Eng. Manuf.*, vol. 227, no. 10, pp. 1430–1441, Oct. 2013.

[21] P. Kyratsis, A. Markopoulos, N. Efkolidis, V. Maliagkas, and K. Kakoulis, "Prediction of thrust force and cutting torque in drilling based on the response surface methodology," *Machines*, vol. 6, no. 2, p. 24, Jun. 2018.

[22] W. Ji and L. Wang, "Industrial robotic machining: A review," *Int. J. Adv. Manuf. Technol.*, vol. 103, nos. 1–4, pp. 1239–1255, Jul. 2019.

[23] Y. Bu, W. Liao, W. Tian, J. Zhang, and L. Zhang, "Stiffness analysis and optimization in robotic drilling application," *Precis. Eng.*, vol. 49, pp. 388–400, Jul. 2017.

[24] J. Jiao, W. Tian, L. Zhang, B. Li, J. Hu, Y. Li, D. Li, and J. Zhang, "Variable stiffness identification and configuration optimization of industrial robots for machining tasks," *Chin. J. Mech. Eng.*, vol. 35, no. 1, pp. 1–16, Dec. 2022, doi: 10.1186/S10033-022-00778-1.

[25] J. Zhang, W. Liao, Y. Bu, W. Tian, and J. Hu, "Stiffness properties analysis and enhancement in robotic drilling application," *Int. J. Adv. Manuf. Technol.*, vol. 106, nos. 11–12, pp. 5539–5558, Feb. 2020.

[26] S. Garnier, K. Subrin, and K. Waiyagan, "Modelling of robotic drilling," in *Proc. 16th CIRP Conf. Modeling Mach. Oper.*, Jun. 2017, pp. 416–421.

[27] B. R. So, B.-J. Yi, and S. Y. Han, "Comparison of impulses experienced on human joints walking on the ground to those experienced walking on a treadmill," *Int. J. Control Autom. Syst.*, vol. 6, no. 2, pp. 243–252, Apr. 2008.

[28] A. Imran and B.-J. Yi, "A closed-form analytical modeling of internal impulses with application to dynamic machining task: Biologically inspired dual-arm robotic approach," *IEEE Robot. Autom. Lett.*, vol. 3, no. 1, pp. 442–449, Jan. 2018.

[29] J. H. Lee, B.-J. Yi, S.-R. Oh, and I. H. Suh, "Performance analysis of sawing based on impulse measure and geometry—Dublahal arm approach," *IEEE Trans. Robot.*, vol. 21, no. 6, pp. 1230–1240, Dec. 2005.

[30] A. Imran and B.-J. Yi, "Impulse modeling and analysis of dual arm hammering task: human-like manipulator," in *Proc. IEEE/RSJ Int. Conf. Intell. Robots Syst. (IROS)*, Oct. 2016, pp. 362–367.

[31] A. Imran and B. J. Yi, "Impulse modeling and new impulse measure for human-like closed-chain manipulator," *IEEE Robot. Autom. Lett.*, vol. 1, no. 2, pp. 868–875, Jul. 2016.

[32] R. Rosen, G. Von Wichert, G. Lo, and K. D. Bettenhausen, "About the importance of autonomy and digital twins for the future of manufacturing," *IFAC-PapersOnLine*, vol. 48, no. 3, pp. 567–572, 2015.

[33] S. Liu, Y. Lu, P. Zheng, H. Shen, and J. Bao, "Adaptive reconstruction of digital twins for machining systems: A transfer learning approach," *Robot. Comput.-Integr. Manuf.*, vol. 78, Dec. 2022, Art. no. 102390.

[34] F. Tao, B. Xiao, Q. Qi, J. Cheng, and P. Ji, "Digital twin modeling," *J. Manuf. Syst.*, vol. 64, pp. 372–389, Jul. 2022.

[35] R. Söderberg, K. Wärmefjord, J. Madrid, S. Lorin, A. Forslund, and L. Lindkvist, "An information and simulation framework for increased quality in welded components," *CIRP Ann.*, vol. 67, no. 1, pp. 165–168, 2018.

[36] F. Xiang, Z. Zhang, Y. Zuo, and F. Tao, "Digital twin driven green material optimal-selection towards sustainable manufacturing," in *Proc. 52nd CIRP Conf. Manuf. Syst. (CMS)*, Ljubljana, Slovenia, Jun. 2019, pp. 1290–1294.

[37] B. Korth, C. Schwede, and M. Zajac, "Simulation-ready digital twin for realtime management of logistics systems," in *Proc. IEEE Int. Conf. Big Data (Big Data)*, Dec. 2018, pp. 4194–4201.

[38] Y. Liu, J. Jin, P. Ji, J. A. Harding, and R. Y. Fung, "Identifying helpful online reviews: A product designer's perspective," *Comput.-Aided Des.*, vol. 45, no. 2, pp. 180–194, 2013.
[39] R. Stark, T. Damerau, and K. Lindow, "Industrie 4.0—Digital redesign of product creation and production in Berlin as an industrial location," in *The Internet of Things*. Berlin, Germany: Springer Vieweg, 2017, pp. 171–186.
[40] J. Wittenburg, *Dynamics of Systems of Rigid Bodies*, B. G. Teubner, Ed. Stuttgart, Germany: Springer, 1997.
[41] R. M. Brach, *Mechanical Impact Dynamics*. New York, NY, USA: Wiley, 1991.
[42] M. B. Lazar, "Cutting force modeling for drilling of fiber reinforced composites," Ph.D. dissertation, Swiss Federal Inst. Technol. Lausanne, Zürich, Switzerland, 2012.
[43] I. D. Walker, "Impact configurations and measures for kinematically redundant and multiple armed robot systems," *IEEE Trans. Robot. Autom.*, vol. 10, no. 5, pp. 670–683, Oct. 1994.
[44] J. Kim, W. Chung, and Y. Youm, "Normalized impact geometry and performance index for redundant manipulators," in *Proc. Millennium Conf., IEEE Int. Conf. Robot. Automat., Symposia*, Apr. 2000, pp. 1714–1719.
[45] A. Imran and B.-J. Yi, "Motion optimization of human body for impulse-based applications," *Intell. Services Robot.*, vol. 11, no. 4, pp. 323–333, Oct. 2018.
[46] S. Neseli, "Optimization of process parameters with minimum thrust force and torque in drilling operation using Taguchi method," *Adv. Mech. Eng.*, vol. 6, pp. 1–10, Oct. 2014.
[47] A. Çiçek, T. Kıvak, and E. Ekici, "Optimization of drilling parameters using Taguchi technique and response surface methodology (RSM) in drilling of AISI 304 steel with cryogenically treated HSS drills," *J. Intell. Manuf.*, vol. 26, no. 2, pp. 295–305, Apr. 2015.
[48] M. Kurt, E. Bagci, and Y. Kaynak, "Application of Taguchi methods in the optimization of cutting parameters for surface finish and hole diameter accuracy in dry drilling processes," *Int. J. Adv. Manuf. Technol.*, vol. 40, nos. 5–6, pp. 458–469, Jan. 2009.
[49] K. V. Rao and P. B. G. S. N. Murthy, "Modeling and optimization of tool vibration and surface roughness in boring of steel using RSM, ANN and SVM," *J. Intell. Manuf.*, vol. 29, pp. 1533–1543, Oct. 2018.
[50] P. M. Kebria, S. Al-Wais, H. Abdi, and S. Nahavandi, "Kinematic and dynamic modelling of UR5 manipulator," in *Proc. IEEE Int. Conf. Syst., Man, Cybern. (SMC)*, Oct. 2016, Art. no. 004229.
[51] K. Kufieta, "Force estimation in robotic manipulators: Modeling simulation and experiments," M.S. thesis, Dept. Eng. Cybern., NTNU Norwegian Univ. Sci. Technol., Trondheim, Norway, Jan. 2014.

ABID IMRAN received the B.S. degree in mechatronics and control engineering from the University of Engineering and Technology, Lahore, Pakistan, in 2011, and the M.S. degree in electronic systems engineering from Hanyang University, South Korea, in 2019, where he is currently pursuing the Ph.D. degree in electronic systems engineering. From March 2019 to August 2019, he was a Postdoctoral Fellow with the Research Institute of Engineering and Technology, Hanyang University. He is currently an Assistant Professor with the Faculty of Mechanical Engineering, Ghulam Ishaq Khan Institute of Engineering Sciences and Technology (GIKI). His research interests include motion optimization, gripper/hand design, artificial intelligence, bio-inspired manipulators, and impact mechanics.

SANGHWA KIM received the B.S. and M.S. degrees from the Department of Electronic Systems Engineering, Hanyang University, Seoul, Republic of Korea, in 2015 and 2017, respectively. He is currently pursuing the Ph.D. degree with the Department of Electrical and Electronic Engineering, Hanyang University. His research interests include robotic integration, robotic grasping and manipulation, and redundant robot.

JAEHONG WOO received the B.S. degree from the Department of Electronic Information System Engineering, Hanyang University, Ansan, South Korea, in 2011, the M.S. degree from the Department of Electronic, Electrical, Control and Instrumentation Engineering, Hanyang University, Seoul, South Korea, in 2013, and the Ph.D. degree from the Department of Intelligent Engineering, Hanyang University, in 2020. From March 2020 to February 2022, he was a Postdoctoral Fellow with the Research Institute of Engineering and Technology, Hanyang University. He is currently an Assistant Professor with the Department of Robotics and Convergence, Hanyang University. His research interests include haptic device and medical robot.

BYUNG-JU YI (Member, IEEE) received the B.S. degree in mechanical engineering from Hanyang University, Seoul, South Korea, in 1984, and the M.S. and Ph.D. degrees in mechanical engineering from The University of Texas at Austin, Austin, TX, USA, in 1986 and 1991, respectively.

From January 1991 to August 1992, he was a Postdoctoral Fellow with the Robotics Group, The University of Texas at Austin. From September 1992 to February 1995, he was an Assistant Professor with the Department of Mechanical and Control Engineering, Korea Institute of Technology and Education, Cheonan, Chungnam, South Korea. In March 1995, he joined the Department of Control and Instrumentation Engineering, Hanyang University. He was a Visiting Professor with Johns Hopkins University, Baltimore, MA, USA, in 2004. He was a JSPS Fellow with Kyushu University, Japan, in 2011. He is currently a Professor with the School of Electrical Engineering, Hanyang University. His research interests include general robot mechanics with application to surgical robotic systems (ENT, neurosurgical, and needle insertion areas), deep learning-based robotic manipulation, and ubiquitous sensor network-based robotics. He is a member of the IEEE Robotics and Automation Society. From 2005 to 2008, he was an Associate Editor of the IEEE Transactions on Robotics. He is also the President-Elect of the Korean Robotics Society and the Korean Society of Medical Robotics.